Journal of Alloys and Compounds 509 (2011) 1373–1377

Contents lists available at ScienceDirect

Journal of Alloys and Compounds

journal homepage: www.elsevier.com/locate/jallcom

Size effects and interactions in $La_{0.7}Ca_{0.3}MnO_3$ nanoparticles

D.H. Manh[a,*], P.T. Phong[b], T.D. Thanh[a], D.N.H. Nam[a], L.V. Hong[a], N.X. Phuc[a]

[a] Institute of Materials Science, Vietnam Academy of Science and Technology, 18 Hoang Quoc Viet Road, Cau Giay Distr., Ha Noi, Viet Nam
[b] Nha Trang Pedagogic College, Khanh Hoa Province, Viet Nam

ARTICLE INFO

Article history:
Received 18 August 2010
Received in revised form 4 October 2010
Accepted 6 October 2010
Available online 3 November 2010

Keywords:
Nanoparticle systems
Surface magnetism
Spin waves
Manganite
$La_{0.7}Ca_{0.3}MnO_3$
Surface effects
Size effects

ABSTRACT

$La_{0.7}Ca_{0.3}MnO_3$ (LCMO) nanoparticles with average diameter of 16–73 nm were prepared by reactive milling and thermal processing methods. Interaction and size effects on the magnetic properties of the LCMO nanoparticle samples were investigated. Phenomena related to the interparticle interaction, such as an un-overlapping of the $M(H_{ext},T)/M_S$ vs. H_{ext}/T scaling plots and a Curie–Weiss rather than Curie law behavior of the dc susceptibility at high temperatures were analyzed. The magnetization curves of interacting nanoparticles were well described by using the mean-field approximation. The dependence of the blocking temperature T_B on the strength of the interactions, magnetic anisotropy, as well as the thermal dependence of magnetization deviates from the expected Bloch law was also estimated.

1. Introduction

Magnetic nanoparticle systems are important for potential applications in magnetic memory devices, refrigeration, sensors, biology, medicine, catalysts [1–5] and have been the subject of intensive research from both the fundamental and application points of view. The remarkable new phenomena observed in nanomaterials arise from the finite-size effects and the interparticle interactions [6–8].

The interparticle interactions may strongly modify the magnetic response of magnetic nanoparticle systems, such as the temperature dependence of the dc susceptibility obeying the Curie–Weiss behavior rather than the Curie law at high temperatures, and the deviations from the Langevin behavior (i.e., un-overlapping of the $M(H_{ext},T)/M_S$ vs. H_{ext}/T scaling plots). The situation of interacting superparamagnetic (SPM) nanoparticles of $La_{0.7}Sr_{0.3}MnO_3$ could be well described by using the mean-field approximation with a field correction to the argument of noninteracting SPM Langevin function $L[(H_{ext}+\alpha M)/k_BT]$ [9,10]. The energy barrier coming from the anisotropy contributions of each particle is also modified with interparticle interactions and, for the different interaction limits, the opposite dependence of T_B with the strength of the interactions is predicted [11,12,25].

The magnetic behavior of the particle surface differs from that corresponding to the core [13–15], which usually displays a spin arrangement similar to that of the bulk material. A much higher magnetic disorder is present in the surface, giving rise to magnetic behaviors which cover from that of a dead magnetic layer to that of a spin glass-like. The competition between both magnetic orders – surface and core – determines the ground state of the particle, which can be very far from the simple assumption of a single domain with the perfect magnetic ordering corresponding to the bulk material. Surface effects dominates the magnetic properties of the smallest particles since a decreasing of particle size increases the ratio of surface spins to the total number of spins. The thermal dependence of magnetization deviates from the Bloch's law due to finite size effects at the nanoscale [16,17].

In a previous paper [18], we reported on magnetic properties of LCMO nanoparticles prepared by reactive milling with different milling times and observed a decrease in the blocking temperature T_B with longer milling times. Furthermore, the temperature dependence of magnetization was found to follow a T^{ε} behavior with $\varepsilon = 1.7$, which slightly deviates from the Bloch law. We have also reported the effect of particle size in the range of 16–73 nm on the magnetic, electrical properties and low-field magnetoresistance of LCMO nanoparticle samples [19,20]. In this study, we present a systematic investigation of magnetic characteristics associated with the finite-size effects and the interparticle interactions for the above-mentioned LCMO samples.

* Corresponding author.
E-mail address: manhdh@ims.vast.ac.vn (D.H. Manh).

0925-8388/$ – see front matter © 2010 Elsevier B.V. All rights reserved.
doi:10.1016/j.jallcom.2010.10.104

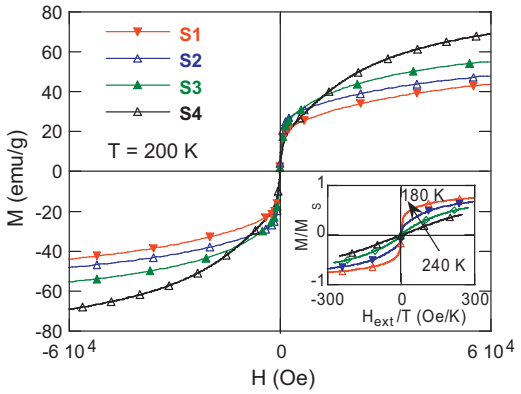

Fig. 1. Anhysteretic curves for all samples with various particle sizes measured at $T = 200$ K. Inset: M/M_S vs. H_{ext}/T curves measured at different temperatures for the sample S4.

2. Experimental

$La_{0.7}Ca_{0.3}MnO_3$ nanoparticles with size in the range of 16–73 nm were prepared by reactive milling and thermal processing methods. The reactive milling is a mechanical alloying process accompanied with solid state reaction to form the desired phase [33,34]. Single phase LCMO powders was obtained after 8 h of milling time in the ambient atmosphere. The powder was then pressed into circular pellets and annealed at 700 °C (S1), 800 °C (S2), 900 °C (S3) and 1000 °C (S4) for 5 h. X-ray diffraction (XRD) measurements were carried out on a SIEMENS D5000 diffractometer. The data were obtained between 20° and 80° 2θ in steps of 0.02° and analyzed using a commercial WIN-CRYSIZE program packet based on the Warren–Averbach formalism. The mean crystallite size of S1, S2, S3, and S4 samples calculated from XRD data is ~16, 35, 43 and 73 nm, respectively (see Ref. [20] for more details). In this report, the particle size will hereafter be referred to as the crystallite size. Magnetic measurements were carried out in a Quantum Design PPMS-6000 in the temperature range of 5–300 K and magnetic fields up to 60 kOe.

3. Results and discussions

Fig. 1 shows the field dependence of magnetization curves $M(H)$ measured at 200 K for all samples with various particle sizes. As seen in figure, the anhysteretic property is observed for all samples. A similar behavior is also observed for $M(H)$ curves measured at temperatures from 180 to 240 K indicating a superparamagnetic (SPM) state for all the samples within this temperature range. However, it is worth noting that the M/M_S vs. H_{ext}/T scaling plots for each sample do not collapse onto a universal magnetization curve as desired for non-interacting SPM systems (see the inset of Fig. 1). The cause for this discrepancy would be the dipolar interaction between the nanoparticles, which leads to a collective contribution to the magnetization. Such a system is usually termed an interacting superparamagnet or interacting nanoparticles assembly [8,10,21].

Moreover, the behavior of interacting nanoparticles is also seen in thermomagnetization measurements. The dc susceptibility deduced from $M_{ZFC}(T)$ in an external field of 10 Oe obeys a Curie–Weiss law, $\chi = C_S/(T - T_0)$, where C_S is a Curie-like constant and the ordering temperature T_0 is determined from the intersection of the linearly extrapolated line $1/\chi(T)$ in the SPM region with T-axis and the value of C_S. Positive T_0 is attributed to ferromagnetic correlations between the particles, the higher T_0 the larger the interaction strength. In some cases, negative values of T_0 have been reported suggesting an antiferromagnetic correlations between the particles [22]. For our samples, T_0 increases monotonically in the temperature range from 211 K to 249 K (Table 1) as the particle size increases.

In order to gain deeper understanding into the magnetization mechanism of the nanoparticle systems, the isothermal field dependence of magnetization were analyzed in terms of the so-called "law of approach to saturation" of an assembly of particles

Table 1
Ordering temperature T_0, blocking temperature T_B and diameter values for all samples determined from Eqs. (4) and (5).

Samples	d_{total} (nm)	d_c (nm)	d_s (nm)	T_0 (K)	T_B (K)
S1	16	13	3	211.5	147
S2	35	31	4	247.9	138
S3	43	39	4	248.1	132
S4	73	68	6	248.9	116

[26]:

$$M(H) = M_S\left[\frac{1 - a/H - b}{H^2 - c/H^3}\right] + \chi_d H \quad (1)$$

where M_S is the saturation magnetization and χ_d is the high-field susceptibility. The best fit of the magnetization curves using Eq. (1) are shown in Fig. 3 for all samples by considering a, b, c and χ_d as free parameters. A rough estimate of the limit of magnetic anisotropy energy in these samples may be obtained by assuming the expression of K_1 for uniaxial anisotropy systems:

$$K_1 = \left[\frac{15}{4} b M_S^2\right]^{1/2} \quad (2)$$

Using the values of b, we obtained very large values of K_1 in range of $0.52–1.14 \times 10^6$ ergs/cm^3, for all the samples at 5 K. The values of K_1 are larger with reducing particle size (Table 2). Similar values of K_1 were reported by Balcells et al. for $La_{2/3}Sr_{1/3}MnO_3$ manganite [23]. The change of K_1 with the particle size is somewhat unexpected since this quantity is only related to the crystal structure of the nanoparticles. However, some factors such as the possible existence of antiferromagnetic clusters and the magnetic frustration due to the disorder and competition of interactions at grain boundaries may have also disturbed the determination of K_1. The contribution of the latter is expected to increase dramatically as particle size decreases. M_S was obtained by means of fitting of result of the field dependence of magnetization measured at 5 K. As shown in Table 2, M_S increases from 65.4 to 86.1 emu/g (i.e., much more smaller than 97.5 emu/g of the bulk [24]) corresponding to increasing particle 16 nm to 73 nm. This lack of saturation is consistent to the core-shelf model for nanoparticles.

Although the $M(H)$ curves can be well fitted to Eq. (1), the M/M_S vs. H/T curves are failed to follow an universal scaling curve, as shown in the inset of Fig. 1, indicating that there perhaps exist significant coupling between the nanoparticles. To better estimate the magnetization curves of these interacting nanoparticles assemblies, we use the mean-field approximation that adds a mean field term $H_{dip} = \alpha M$ to the external field H_{ext} (see Refs. [10,31,32]). The magnetization M, therefore, can be expressed by an *argument-corrected Langevin function*:

$$M(H,T) = M_S L\left(\frac{M_S \bar{m}[H_{ext} + \alpha M(H,T)]}{k_B T}\right) \quad (3)$$

where $L(x)$ is the Langevin function of x, $\bar{m}$ is the average particle mass (in g/cm^3) and M_S was determined by fitting the value of the magnetization measured at 5 K to Eq. (1). The value of C_S was determined by using the experimental data for the initial susceptibility χ at low field. From Eq. (3), χ is expressed as initial slope of the universal curve:

$$\begin{cases} \chi = \dfrac{M_S^2 \bar{m}}{3k_B(T - T_0)} \\ \dfrac{1}{\chi} = \dfrac{1}{C_S}(T - T_0) = \dfrac{1}{C_S}T - \alpha \\ C_S = \dfrac{M_S^2 \bar{m}}{3k_B} \end{cases} \quad (4)$$

Table 2
Particle size, B, ε, K_1 and M_S for all samples.

Sample	Particle size (nm)	$B \times 10^{-5}$ ($K^{-\varepsilon}$)	ε	M_S (emu/g) at 0 K	M_S (emu/g) at 5 K	$K_1 \times 10^6$ (erg cm^{-3})
S1	16	6.73	1.67	65.38	62.68	1.14
S2	35	7.44	1.62	78.04	74.43	1.07
S3	43	9.48	1.61	82.81	82.16	0.73
S4	73	12.39	1.56	86.39	85.08	0.52

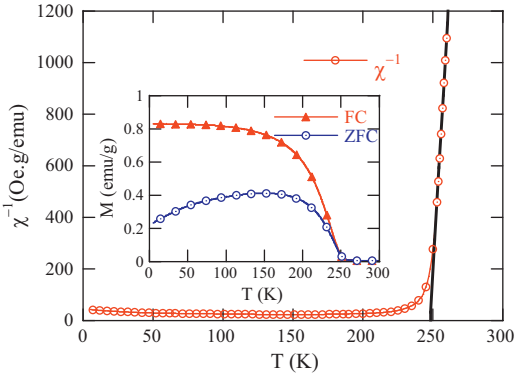

Fig. 2. Inverse dc susceptibility vs. temperature measured at 10 Oe for the sample S1. Inset: temperature dependence of magnetization of sample S1 under *FC* and *ZFC* mode at 10 Oe.

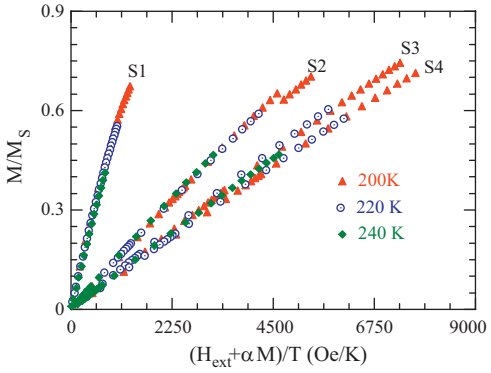

Fig. 4. Scaled magnetization curves M/M_S vs. $(H_{ext} + \alpha M)/T$ for all samples at temperatures 200 K, 220 K and 240 K.

The value of α can be determined by extrapolating the $1/\chi$ vs. T curves as shown in Fig. 2. Two parameters α and M_S are then used to plot the M/M_S vs. $(H_{ext} + \alpha M)/T$ scaling curves at different temperatures for the samples. As expected, the scaled curves overlap into an universal curve characteristic for each sample. The universal scaling magnetization curves for the experimental data of all samples are shown in Fig. 3.

In order to further validate our proposed mean-field approximation to experimental data, it is essential to check the universality of scaled mean-field Lagevin function (we call it *argument-corrected Langevin function*). We inserted $\tilde{m}$ into Eq. (4) and M_S into Eq. (3) and fitted the function with the data of corresponding universal magnetization curves for each sample (see Fig. 4). Fig. 5 shows an example of the best fit for sample S4. The results clearly show that the magnetization curves of interaction LCMO nanoparticles of average diameter 16–73 nm are well described by using the mean-field approximation.

The zero-field-cooled temperature dependence of magnetization of the LCMO nanoparticles is shown in Fig. 6. The blocking temperature T_B of the LCMO nanoparticles decrease from 147 K to 116 K as particle size increases from 16 nm to 73 nm. The inset of Fig. 6 shows a linearly decrease of T_B with particle size. Some authors reported that the blocking temperature T_B decreases nomonotonically as the particle size decreases/or the milling time increases [13,18]. Morup [12] suggested that two magnetic

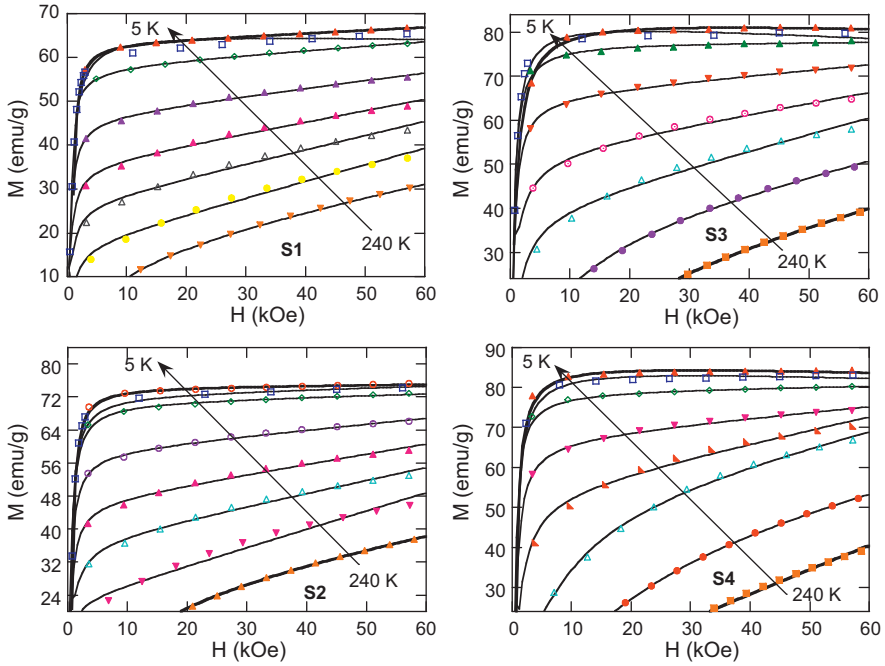

Fig. 3. Isothermal magnetization curves of samples S1, S2, S3, and S4 measured at several temperatures from 5 K to 240 K. The solid lines through the $M(H)$ data correspond to the fits using Eq. (1) in the text.

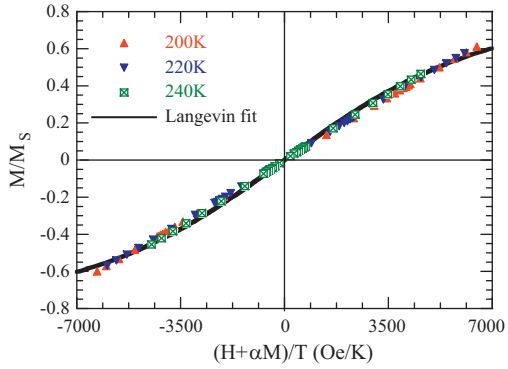

Fig. 5. Scaled magnetization curves for the sample S4. Solid line: the magnetically weighted argument-corrected Langevin function fitting to the scaled data.

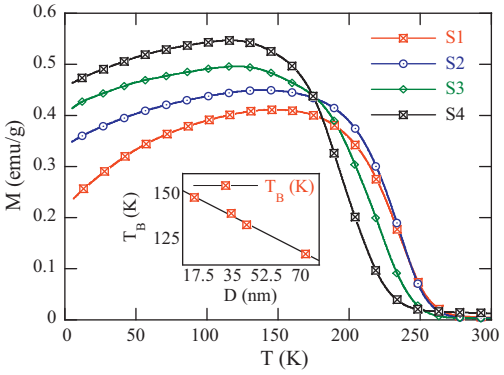

Fig. 6. Temperature dependence of magnetization of LCMO samples under *ZFC* mode at 10 Oe. Inset: particle size dependence of blocking temperature of LCMO samples.

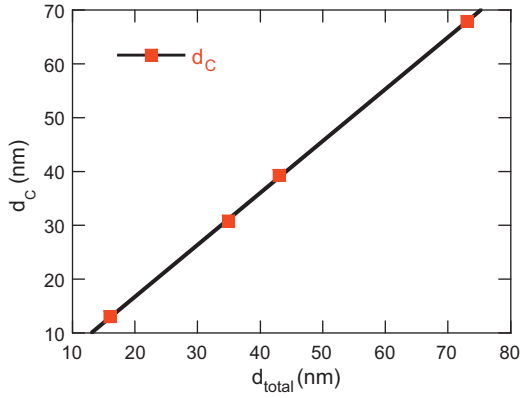

Fig. 7. The core diameter vs. total median diameter calculated using Eq. (5).

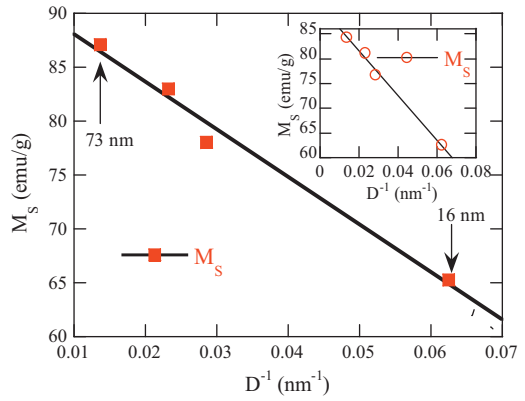

Fig. 8. Saturation magnetization as a function of the surface/volume ratio at 0 K and at 5 K (as shown in the inset). Solid line is the regression fit to the data.

regimes, governed by opposite dependencies of T_B, occurring due to interaction particles. In case of weak interaction, T_B signals the onset of a blocked state and T_B decreases as the interaction increase. In contrast, for strong interaction, a transition occurs from an SPM state to a collective state which shows most of the features of typical glassy behavior. In this case, T_B is associated with a freezing process and it increases with the interactions. The blocking temperature decreases significantly as the interaction strength increases in our experiments (as shown in Table 1). These results are in agreement with the simulations by Berkov and Gorn for strong anisotropy systems [28].

As above-mentioned, the decrease in magnetization with decreasing particle size is related to the higher surface to volume ratio in the smaller particles. The shells are poorly magnetic due to noncollinear spin structures or spin-glass-like disorders [13,15]. A model of the core-shell structure for nanoparticles was proposed by Gangopadhyay et al. [26]. The LCMO particles are assumed to be spherical and to be composed of an ideal single-crystalline core with the saturation magnetization of the core is $M_c = 97.5$ emu/g [24] and the density is $\rho_c = 5.9$ g/cm^3 [27] (such values corresponds to the values of bulk single crystals). For a particle of total radius r, consisting of a core surrounded by a shell of thickness $dr \ll r$ (the corresponding ρ_s value are roughly assigned 4 g/cm^3), the core diameter (d_c) can be calculated by Eq. (5) [26]:

$$d_c = \left\{ \frac{\rho_s/\rho_c}{[(\rho_s/\rho_c)/ + (M_c - M_S)/(M_S - M_{shell})]} \right\}^{1/3} d_{total} \quad (5)$$

Using Eq. (5), we calculated the core diameter (d_c) from particle diameter (d_{total}) with assuming a nonmagnetic shell ($M_{shell} = 0$). Then, d_c was plotted against total diameter, d_{total} (as shown in Fig. 7). From the linear regression fit to the data, the equation of the straight line was found to be as follows:

$$dc = (0.96\, d\,\text{total} - 2.5)\,\text{nm} \quad (6)$$

The nonmagnetic shell thickness increases from 3 nm to 5 nm as the particle diameter increases from 16 nm to 73 nm. Similar results for ultrafine iron particles have been reported by Gangopadhyay et al. [26].

The saturation magnetization at 0 K and 5 K is reduced linearly with the surface/volume ratio (D^{-1}) (see Fig. 8). This result is consistent with that reported by other authors [14,20,26]. This linear dependence of magnetization on the surface/volume ratio (D^{-1}) confirms the suggestion that the magnetization is actually influenced by the surface of the particle.

In recent reports [13,16,17], the temperature dependence of magnetization including finite size effects is given by expression as:

$$M_S(T) = M_S(0)[1 - BT^{\varepsilon}] \quad (7)$$

where $M_S(0)$ is the spontaneous magnetization at 0 K and B is a constant related to the exchange integral, J ($B \sim 1/J^{\varepsilon}$). Eq. (7) is known as the Bloch $T^{3/2}$ law with $\varepsilon = 3/2$ which has been verified experimentally for most of the bulk materials [29]. However, in nanoparticles, the thermal dependence of magnetization deviates from the expected Bloch law as the magnons with wavelength larger than the particle diameter cannot be excited and a threshold of thermal energy is required to generate spin waves [7,30]. Moreover, the values of ε depend on size, size distribution, shape and different magnetic assemblies such as the different values of ε were reported for some of the bulk spinel ferrites [30].

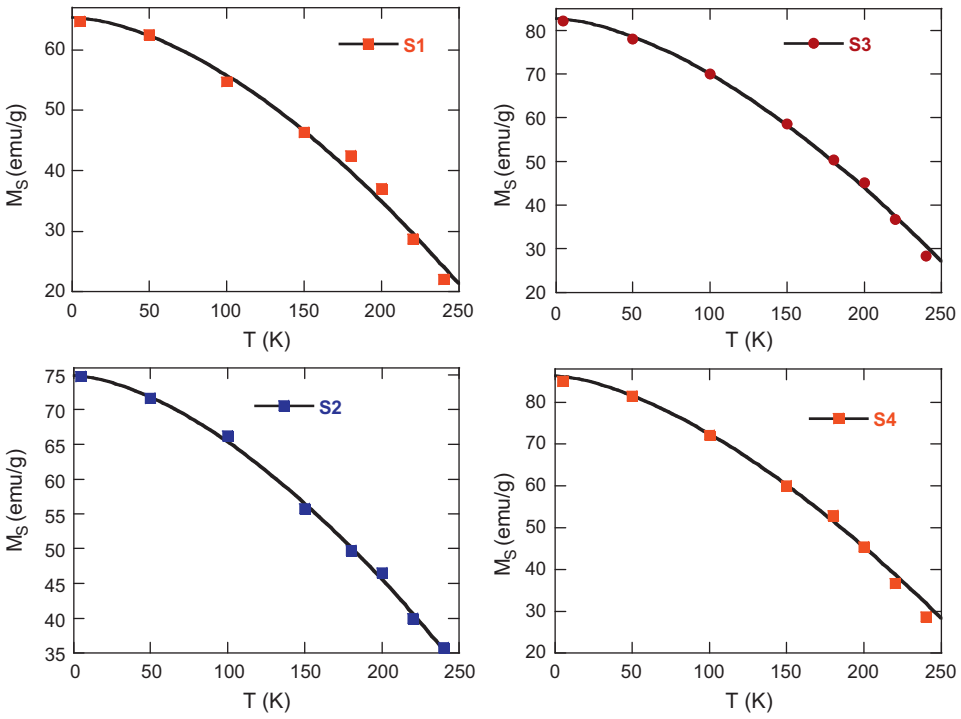

Fig. 9. Saturation magnetization as a function of temperature for all samples. Solid curve is power law fitted with the form $M_S = M_0(1 - BT^{\varepsilon})$ to the data points.

Some theoretical calculations as well as experiment results for nanoparticles and clusters have shown a wide range of the value of ε between 0.3 and 2 [6].

We have also performed isothermal magnetization measurements as a function of magnetic field at different temperatures (see Fig. 3). The temperature dependence of saturation magnetization for all samples is shown in Fig. 9. The M_S values is obtained by fitting the magnetization curves by Eq. (1) (see Fig. 3). A fit to the saturation magnetization data by Eq. (7) is presented in Fig. 9 (solid curve). As seen in Table 2, the values of $M_S(0)$ and B increase as particle size increases, while the value of ε decreases and it is close with the value of $\varepsilon = 3/2$ of bulk materials [29].

4. Conclusion

In summary, the magnetic characteristic and analysis have been done for $La_{0.7}Ca_{0.3}MnO_3$ nanoparticles with average particle size from 16 nm to 73 nm fabricated by reactive milling and thermal processing methods. Magnetic measurements showed the existence of magnetic interaction between particles. A mean field approximation can describe well magnetic behavior of interacting nanoparticle assemblies. The blocking temperature decreases with the increase of interaction strength or particle size, which are suggested to be due to contribution of strong magnetic anisotropy. The reduction of saturation magnetization with surface/volume ratio is mainly due to the formation of a nonmagnetic surface shell around the nanoparticles. The temperature dependence of magnetization based on a thermal distribution of spin waves and fit results to a power law T^{ε} showed that ε decreases from 1.67 to 1.56 as the particle size increases from 16 to 73 nm.

Acknowledgments

This work was supported by the National Foundation for Science and Technology grant No.103.02.48.09. The authors are also thankful to the IMS National Key Laboratory for Electronic and Devices. The second author would like to thank Nhatrang Pedagogic College.

References

[1] J.L. Dormann, D. Fiorani, E. Tronc, Adv. Chem. Phys. 98 (1997) 283.
[2] J.F. Bobo, L. Gabillet, M. Bibes, J. Phys.: Condens. Matter 16 (2004) S471.
[3] Q.A. Pankhurst, J. Connolly, S.K. Jones, J. Dobson, J. Phys. D: Appl. Phys. 36 (2003) R167.
[4] A.G. Roca, R. Costo, A.F. Rebolledo, S.V. Verdaguer, P. Tartaj, T. Gonzalez-Carreno, M.P. Morales, C.J. Serna, J. Phys. D: Appl. Phys. 42 (2009) 224002.
[5] B. Seyfi, M. Baghalha, H. Kazemian, Chem. Eng. J. 148 (2009) 306.
[6] R.H. Kodama, J. Magn. Magn. Mater. 200 (1999) 359.
[7] X. Batlle, A. Labarta, J. Phys. D: Appl. Phys. 35 (2002) R15.
[8] S.A. Majestich, M. Sachan, J. Phys. D: Appl. Phys. 39 (2006) R407.
[9] N.X. Phuc, Ha.M. Nguyen, D.H. Manh, L.T. Hung, L.T.C. Tuong, L.V. Hong, Y.-D. Yao, J. Magn. Magn. Mater. 304 (2006) 133.
[10] N.M. Ha, D.H. Manh, L.V. Hong, N.X. Phuc, J. Korean Phys. Soc. 52 (2008) 1447.
[11] S. Morup, E. Tronc, Phys. Rev. Lett. 72 (1994) 3278.
[12] S. Morup, Europhys. Lett. 28 (1994) 671.
[13] S. Roy, I. Dubenko, D.D. Edorh, N. Ali, J. Appl. Phys. 96 (2004) 1202.
[14] M.A. Lopez-Quintela, L.E. Hueso, J. Rivas, F. Rivadulla, Nanotechnology 14 (2003) 212.
[15] P. Dey, T.K. Nath, P.K. Manna, S.M. Yusuf, J. Appl. Phys. 104 (2008) 103907.
[16] K. Mandal, S. Mitra, P. Anil Kumar, Europhys. Lett. 75 (2006) 618.
[17] K. Maaz, A. Mumtaz, S.K. Hasanain, M.F. Bertinoc, J. Magn. Magn. Mater. 322 (2010) 2199.
[18] Do.H. Manh, N. Chi Thuan, P. Thanh Phong, L. Van Hong, N. Xuan Phuc, J. Alloys Compd. 479 (2009) 828.
[19] D.H. Manh, P.T. Phong, T.D. Thanh, L.V. Hong, N.X. Phuc, J. Alloys Compd. 499 (2010) 131.
[20] D.H. Manh, P.T. Phong, T.D. Thanh, L.V. Hong, N.X. Phuc, J. Alloys Compd. 491 (2010) 8.
[21] P. Allia, M. Coisson, P. Tiberto, F. Vinai, M. Knobel, M.A. Novak, W.C. Nunes, Phys. Rev. B 64 (2001) 144420.
[22] X.X. Zhang, G.H. Wen, G. Xiao, S. Sun, J. Magn. Magn. Mater. 261 (2003) 21.
[23] L.L. Balcells, J. Fontcubrta, B. Martinez, X. Obradors, J. Phys.: Condens. Matter 10 (1998) 1883.
[24] H. Song, W. Kim, S.-J. Kwon, J. Appl. Phys. 89 (2001) 3398.
[25] M. García del Muro, X. Batle, A. Labarta, J. Magn. Magn. Mater. 221 (2000) 26.
[26] S. Gangopadhyay, G.C. Hadjipanayis, B. Dale, C.M. Sorensen, K.J. Klabunde, V. Papaefthymiou, Phys. Rev. B 45 (1992) 9778.
[27] H.A. Alwi, Abd-Shukor, IEEE Trans. Magn. 45 (2009) 2899.
[28] D.V. Berkov, N.L. Gorn, J. Phys.: Condens. Matter 13 (2001) 9369.
[29] M. Thakur, K. De, S. Giri, S. Si, A. Kotal, T.K. Mandal, J. Phys.: Condens. Matter 18 (2006) 9093.
[30] P.V. Hendriksen, S. Lenderoth, P.A. Lindgard, Phys. Rev. B 48 (1993) 7259.
[31] L. Wang, J. Ding, Y. Li, Y.P. Feng, N.X. Phuc, N.H. Dan, J. Appl. Phys. 89 (2001) 8046.
[32] Y. Shi, J. Ding, J. Appl. Phys. 90 (2001) 4078.
[33] G. Jangg, F. Kuttner, F. Korb, Aluminum 51 (1975) 641.
[34] S. Kaliaguine, A. Van Neste, V. Szabo, J.E. Gallot, M. Bassir, R. Muzychuk, Appl. Catal. A: Gen. 209 (2001) 345.